Available online at www.sciencedirect.com
SCIENCE DIRECT®
Journal of Magnetism and Magnetic Materials 301 (2006) 532–540
www.elsevier.com/locate/jmmm

A novel configuration for a brushless DC motor with an integrated planetary gear train

Hong-Sen Yan*, Yi-Chang Wu

Department of Mechanical Engineering, National Cheng Kung University, Tainan 70101, Taiwan, ROC

Received 1 August 2004; received in revised form 17 March 2005
Available online 6 September 2005

Abstract

This paper presents a novel configuration of a brushless DC (BLDC) motor with an integrated planetary gear train, which provides further functional and structural integrations to overcome inherent drawbacks of traditional designs. The effects of gear teeth on the magnetic field and performance of the BLDC motor are investigated. Two standard gear profile systems integrated on the stator with feasible numbers of gear teeth are introduced to reduce the cogging torque. An equivalent magnetic circuit model and an air-gap permeance model are applied to analytically analyze the magnetic field, while the validity is verified by 2-D finite-element method (FEM). Furthermore, the motor performance is discussed and compared with an existing design. The results show that the present design has the characteristics of lower cogging torque and torque ripple than the conventional design, which is of benefit to the widely applications on accurate motion and position control for BLDC motors.

PACS: 84.50.+d

Keywords: Novel motor configuration; Brushless DC motor; Planetary gear train; Cogging torque reduction; Magnetic circuit analysis

1. Introduction

It is well known that electric motors and gear reducers are commonly the component devices of the present day machinery. These two devices, in general, are connected to provide functions of power generation and transmission, which are widely used in high driving torque and/or low rotational speed applications, e.g., cordless power tools, electric transporters, office automation apparatuses, and factory conveying equipments, etc. Traditionally, electric motors and gear reducers are independently designed and manufactured, and matched appropriately for transforming speed and torque to meet needed driving requirements. Intermediary mechanical components such as couplings or power-transmitting elements are further employed for the purpose of transmitting motion and energy from the electric motor to the gear reducer. Fig. 1 shows the schematic diagram of a typical design, in which a brushless DC (BLDC) motor is connected with a gear reducer by bolts. The shaft of the BLDC motor integrated with a helical gear is in mesh with a gear train of the gear reducer. Since the efficiency of the electric motor is related to its rotational speed, the main advantage of such a conventional design is the capability of operating in motor's most efficient state, because the output speed is mechanically reduced. However, it inherently suffers from two significant disadvantages. One is the additional mechanical loss caused by the friction of intermediary mechanical components, which results in undesirable low efficiency. The other is the redundant mechanical elements usage and incompact workspace arrangements due to individual designs of the electric motor and the gear reducer. This not only increases the manufacturing and the maintenance cost, but also makes it difficult to reduce the overall size. Therefore, the development of integrating gear reducers within electric motors to overcome the above shortcomings is becoming increasingly important.

During the recent years, there has been a growing interest in the integrated design of electric machines with

*Corresponding author. Tel.: +886 6 208 2703; fax: +886 6 208 4972.
E-mail address: hsyan@mail.ncku.edu.tw (H.-S. Yan).

0304-8853/$ - see front matter © 2005 Elsevier B.V. All rights reserved.
doi:10.1016/j.jmmm.2005.07.031

Nomenclature

A	addendum of the gear teeth
$B(\phi)$	flux density of the air gap without considering the stator slots
$B_g(\theta, \phi)$	magnetic flux density of the air gap
$B_{g,ave}$	average flux density within the air gap
B_r	magnet residual flux density
D	dedendum of the gear teeth
D_i	inner stator diameter
$E_g(\theta)$	air-gap stored energy
g_e	effective air-gap length
i_{ph}	phase current
K_e	back-EMF constant
K_l	correction factor due to losses
K_w	winding factor
L	stack length
l_m	magnet height
M	gear module
m	phases of conduction
N	total conductors per phase
N_t	number of teeth spaces associated with one magnet pole
n_c	number of coils
P	number of magnet poles
R_g	air-gap reluctance associated with one magnet pole
R_{mo}	reluctance of a magnet
R_{ro}	outside rotor radius
S	number of armature slots
T	number of gear teeth
T_{ave}	average electromagnetic torque
$T_c(\theta)$	cogging torque
$v(\phi)$	volume function
w	width of the tooth space
η	reluctance ratio of a magnet pole to the magnet-to-rotor leakage flux
θ	rotor position
λ	reluctance ratio of a magnet pole to the magnet-to-magnet leakage flux
μ_o	permeability of air
μ_r	relative permeability of the magnet
τ_f	length of two adjacent magnets
τ_m	magnet width
ϕ	arbitrary angle in the air gap

the corresponding driven devices, such as the integration of starters and generators used in hybrid vehicles [1], the integration of electric motors and steering assemblies used in vehicle power steering systems [2], and the integration of electric motors, pumps, and controllers used in automotive water pump applications [3], etc. Such integrated devices offer new opportunities for improving system performances and/or reducing manufacturing costs. In contrast, the integration of electric motors and gear reducers has received relatively little attention. An examination of the existing products and related patents [4,5] reveals that most of them focus only on connecting casings of gearboxes to stators of electric motors. Novel concepts providing further functional and structural integrations to surmount inherent drawbacks are not proposed. Moreover, literature in effects of mechanical elements of the gear reducer on the magnetic field of the electric motor is still not available.

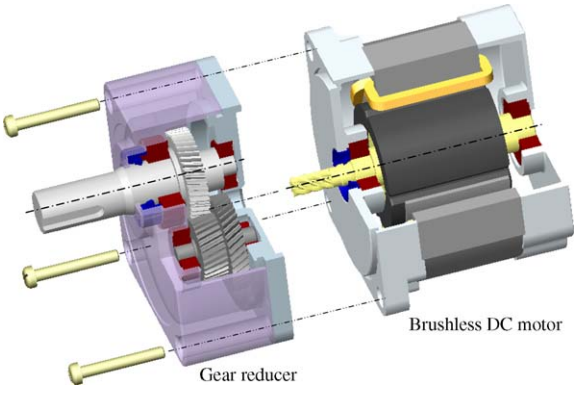

Fig. 1. Conventional design of a BLDC motor connected with a gear reducer.

Based on the above reasoning, the objective of this paper is to propose an innovative concept by integrating a planetary gear train within a BLDC motor to be a compact structural assembly. In what follows, the motor configuration and its features are presented first. The influence of gear teeth on the magnetic field and motor performance of the BLDC motor is studied. From the Fourier expansion of the air-gap flux density, the relationships to the number of gear teeth, the number of magnet poles, and the orders of dominant harmonic components of the cogging torque are investigated. Two standard gear profile systems with feasible numbers of gear teeth integrated on the stator are provided for reducing the cogging torque. Then, the equivalent magnetic circuit method is employed to derive analytical expressions for calculating the average flux density within the air gap, back-EMF constant, and electromagnetic torque. Six numerical cases of the proposed motor configuration are illustrated, and the accuracy is also verified by the finite-element method (FEM). Finally, the motor performance is discussed and compared with an existing design.

2. Motor configuration

Fig. 2 shows the configuration of the novel concept, where a planetary gear train is integrated and embedded within a 4-pole/6-slot, interior-rotor BLDC motor. The planetary gear train with a two-stage reduction structure is provided due to the advantages of compactness, lightweight,

and high gear ratio compared with other kinds of gear reducers. It consists of a sun gear (member 1), a sun gear integrated with a carrier (member 2), a ring gear (member 3), a carrier (member 4), and two planet gears (members 5 and 6), as shown in Fig. 3. Each of members 5 and 6 employ two planet gears to mesh with the ring gear in order to provide better balancing of gear tooth loads and inertia forces. According to the structural characteristics, members 1, 2, 3, and 4 of the planetary gear train are all coaxial with the rotor and stator of the BLDC motor, three of them can be employed as the input, output, and ground terminals, respectively, for the purpose of transmission. Furthermore, it is attractive to integrate the gear elements of the planetary gear train with motor components of the BLDC motor due to their coaxial relationships. In this concept, the sun gear (member 1) is the input terminal, which is combined with the rotor. The carrier is the output terminal, which is connected to the output shaft of the integrated design. The ring gear is the ground terminal, where the geometry of the internal gear teeth is integrated on the surfaces of stator pole shoes facing the permanent magnets, as shown in Fig. 4. Each slot opening of the stator is formed by removing the bottom land of the ring gear, which enables the copper conductors to set into the slot areas, and also does not affect the conjugate relation for gear meshing. Unlike the traditional manufacturing process of cut gears, the ring gear integrated on the stator comprises a lamination of plural steel slices. The fine-blanking process, which is a precision-punching method, forms those slices of the ring gear and the stator by using the identical punching die. There are several convex portions on one side of the punched steel plate and corresponding concave portions on the other side. The convex and concave portions between adjacent punched plates are engaged in the form of interference fit, so that punched plates can be firmly locked and integrally coupled in the axial direction without using any mechanical fastener. In assembly, those slices engaged with planet gears have a 90° mechanical angle shift along the center axis with respect to others, which makes the end-turns of the copper windings to accommodate inside the slot areas.

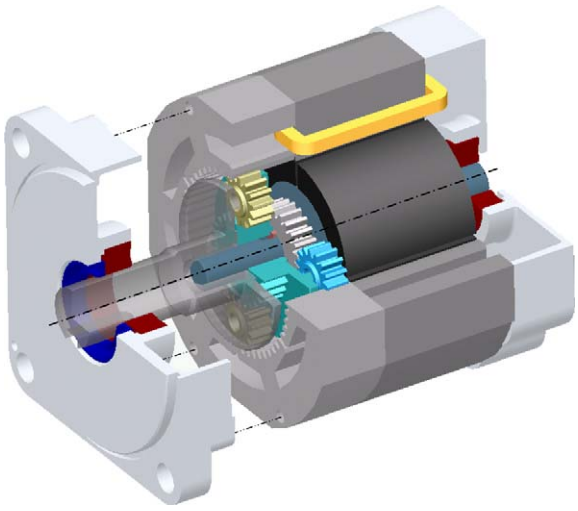

Fig. 2. Configuration of the proposed BLDC motor integrated with a planetary gear train.

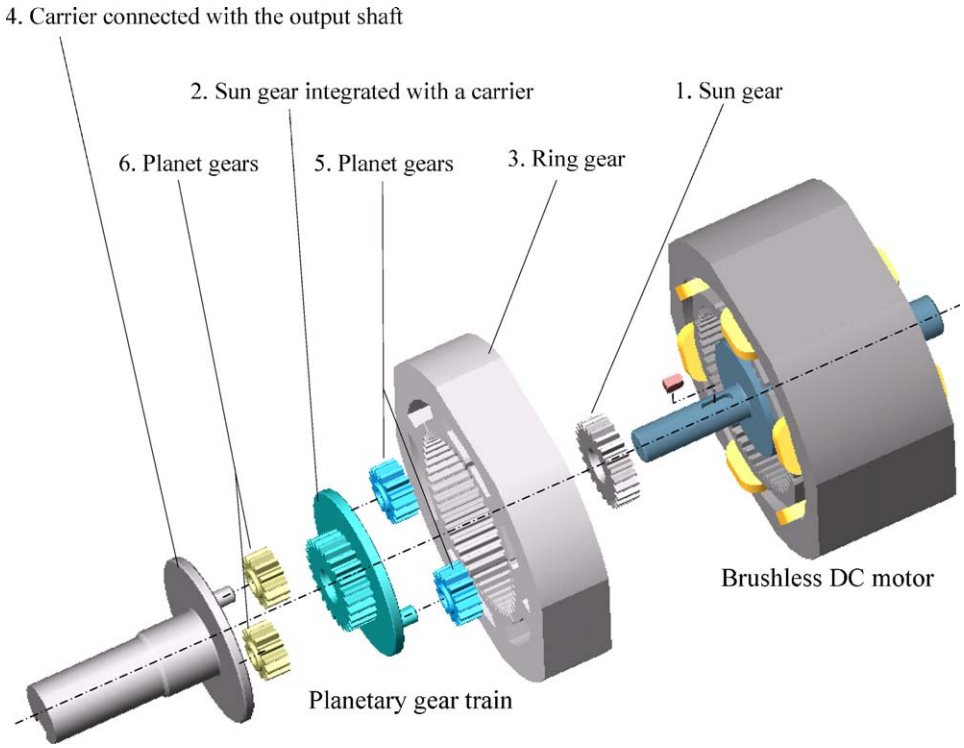

Fig. 3. Exploded view of the planetary gear train.

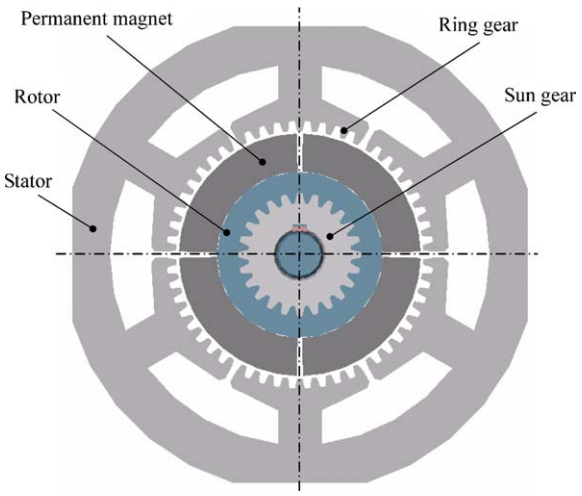

Fig. 4. Cross-section of the proposed concept.

In contrast to conventional designs, the main features of the proposed motor configuration include:

(1) The BLDC motor with an integrated planetary gear train reduces the use of couplings, the casing of the gearbox, and corresponding bolts or fasteners, which makes the whole configuration more compact, light-weight, and easier for maintenance.
(2) Motor components combined with gear elements make it attractive to simplify the mechanisms and reduce the overall size especially in the axial direction. It also shrinks the length of the power flow path from the electric motor to the gear reducer, and hence decreases the mechanical losses caused by the friction.
(3) The output shaft of the gear reducer and the shaft of the electric motor usually are not coaxial for traditional designs, as shown in Fig. 1. In this concept, the rotor, stator, and most rotary components of the planetary gear train are all coaxial with the output shaft, while the balanced planet gears are also employed. It may possess better characteristics on dynamic balance than traditional designs.
(4) The gear teeth integrated on the stator provide functions not only for transmission, but also act as dummy slots [6] for reducing the cogging torque of the BLDC motor. It is of benefit to the widely applications on accurate motion and position control for BLDC motors.

3. Cogging torque analysis

For brushless permanent-magnet motors, the cogging torque arises from the interaction of permanent magnets and the stator-slotted structure without the applied driving current. It may induce vibration, acoustic noise, and possible resonance particularly at high load and low speed. Since the cogging torque is greatly affected by the configuration of the stator, the prediction of the cogging torque for the proposed motor becomes an essential task. In this section, the effects of gear teeth on the cogging torque are studied. Also, standard gear profile systems with feasible numbers of gear teeth on the stator for cogging torque reduction are discussed.

In a permanent magnet motor, the energy is stored in the air gap, the iron core, and the permanent magnets. However, the energy change in permanent magnets and iron core, in general, is negligible compared to that of air [7]. Therefore, according to the principle of virtual work, the cogging torque, $T_c(\theta)$, can be estimated by calculating the rate of change of the stored energy in the air gap, $E_g(\theta)$, with respect to the rotor position, θ, and is expressed as

$$T_c(\theta) = \frac{-\partial E_g(\theta)}{\partial \theta}, \tag{1}$$

where

$$E_g(\theta) = \int_0^{2\pi} \frac{1}{2\mu_0} B_g^2(\theta, \phi) v(\phi)\, d\phi, \tag{2}$$

where μ_0 is the permeability of air, ϕ is an arbitrary angle in the air gap, $B_g(\theta,\phi)$ is the magnetic flux density of the air gap, and $v(\phi)$ is the volume function which is usually approximated as a constant [8]. Since the tooth space between two adjacent gear teeth is a slot portion on the stator, as shown in Fig. 5(a), the presence of one tooth space at the position α_m can be defined as

$$\begin{aligned} u(x-\alpha_m) &= 1 \quad \text{when } |x-\alpha_m| \leqslant w/2, \\ u(x-\alpha_m) &= 0 \quad \text{when } |x-\alpha_m| > w/2, \end{aligned} \tag{3}$$

where w is the width of the tooth space measured along the pitch circle of the ring gear. Hence, the presence of the tooth spaces on the stator, as shown in Fig. 5(b), is expressed as

$$u_t(\theta, \phi) = \sum_{m=1}^{T} u\left(\phi - \theta - \frac{2\pi}{T} m\right), \tag{4}$$

where T is the number of gear teeth of the ring gear integrated on the stator. For simplicity, the air-gap

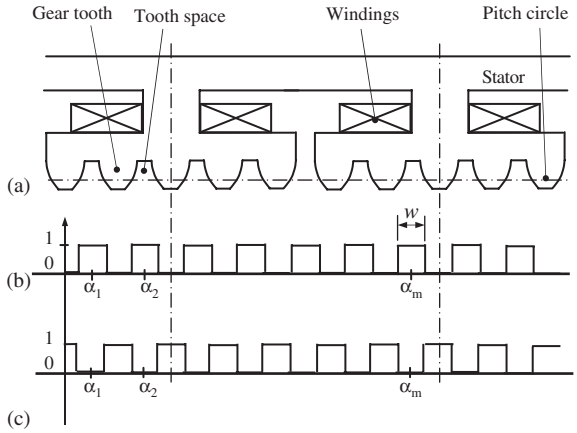

Fig. 5. Representation of the presence of the tooth spaces and the corresponding permeance function.

permeance function is assumed to be a simple unit function [9], as shown in Fig. 5(c), and the magnetic flux density of the air gap can be written as

$$B_g(\theta,\phi) = [1 - u_t(\theta,\phi)]B(\phi), \tag{5}$$

where $B(\phi)$ represents the magnetic flux density of the air gap when the stator has no slot, which is defined by the distribution of the residual magnetic flux density of the permanent magnets [8]. It can be expressed using Fourier expansion as follows:

$$B(\phi) = \sum_{n=1}^{\infty} B_n \sin\left(\frac{nP\phi}{2}\right), \tag{6}$$

and

$$B^2(\phi) = A_0 + \sum_{n=1}^{\infty} A_n \cos(nP\phi), \tag{7}$$

where P is the number of magnet poles, A_0 is the DC component of $B^2(\phi)$, A_n and B_n are the coefficients of the nth harmonic components of $B^2(\phi)$ and $B(\phi)$. In addition, based on the mean value theorem for definite integrals, the following equation is established:

$$\int_0^{2\pi} B^2(\phi)u_t(\theta,\phi)\,d\phi = w\sum_{m=1}^{T} B^2\left(\theta + \frac{2\pi}{T}m\right). \tag{8}$$

Substituting Eqs. (2), (4), (5), (7), and (8) in Eq. (1), the cogging torque, $T_c(\phi)$, becomes

$$T_c(\theta) = K\sum_{n=1}^{\infty} nA_n \sum_{m=1}^{T} \sin nP\left(\theta + \frac{2\pi}{T}m\right), \tag{9}$$

where K is a constant. It can be seen from Eq. (9) that some harmonic components of the cogging torque are automatically eliminated due to the specific relationships of the number gear teeth and magnet poles

$$\sum_{m=1}^{T} \sin nP\left(\theta + \frac{2\pi}{T}m\right) = 0 \quad \text{when} \quad \frac{nP}{T} \notin N. \tag{10}$$

In other words, the nth harmonic components that cause the cogging torque is then given by

$$n = i\frac{T}{\gcd(P,T)}, \quad i = 1,2,3,\ldots, \tag{11}$$

where $\gcd(P,T)$ is the greatest common divisor of P and T. According to Eq. (11), the order of the harmonic components that dominate the cogging torque is mainly related to the number of gear teeth on the stator and the number of permanent magnets on the rotor. For a conventional 4-pole/6-slot BLDC motor, the number of stator teeth is equal to 6, and the dominant harmonic components of the cogging torque are of order $3i$ ($i = 1, 2, 3, \ldots$). As 42 gear teeth are placed at regular intervals on the stator of this motor, for example, the first 20 harmonic components of the cogging torque disappear, i.e., the harmonic components that generate the cogging torque turn into order $21i$. Since the magnitude of the harmonic component usually decreases in accordance with the increase of its order number, the implementation for cogging torque reduction is to make the dominant harmonic components with higher order numbers. Table 1 shows the nth harmonic components that generate the cogging torque of a 4-pole/6-slot BLDC motor, and three different numbers of gear teeth integrated on the stator of this motor. Due to the influence of tooth spaces on the stator, it shows that the orders of dominant harmonic components of the cogging torque for the proposed designs are all higher than the conventional design. In this work, two commonly used standard gear profile systems, i.e., the 14.5° full-depth involute system and the 20° stub-tooth involute system [10], are employed. In order to design with similar motor dimensions, the number of gear teeth is appropriately matched with the standard gear module, so that the inner stator diameter, D_i, is close to that of 53 mm for an existing 4-pole/6-slot BLDC motor. Some of the more important terms and dimensions associated with these two systems are shown in Fig. 6 and Table 2. The commercial finite-element package Ansoft/Maxwell is applied to calculate the cogging torque and also to verify the accuracy of the magnetic circuit analysis presented in the next section. For making a quantitative comparison, motor parameters including: the stator outside diameter of 97 mm and the stack length of 43 mm that govern the sizing equation, the air-gap length of 0.5 mm, and the ferrite magnet with a remanence of 0.16 T, a relative permeability of 1.05, and a thickness of 8 mm, are defined to be identical with the existing product. As illustrated in Fig. 7, it is found that the cogging torque

Table 1
The nth harmonic components that generate the cogging torque

P	S[a]	T	gcd (P, T)	n
4	6	—	2	$3i$
4	6	42	2	$21i$
4	6	54	2	$27i$
4	6	66	2	$33i$

[a] S is the number of armature slots.

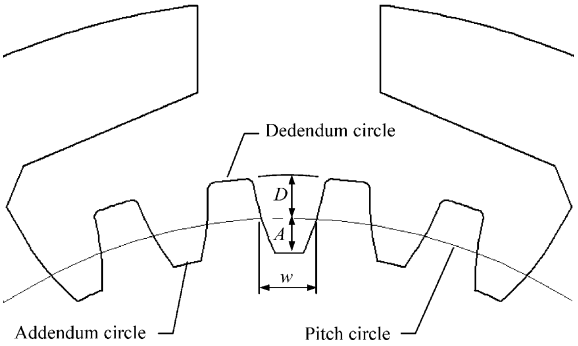

Fig. 6. Addendum (A), dedendum (D), and tooth thickness (w) of the internal gear teeth on the stator.

Table 2
Some important terms and dimensions associated with the standard gear profile systems integrated on the stator

System	Case	T	M[a]	A (mm)	D (mm)	w (mm)	D_i[a] (mm)
14.5° full-depth involute	I	42	1.25	1.25	1.45	1.96	50
	II	54	1	1	1.16	1.57	52
	III	66	0.8	0.8	0.93	1.26	51.2
20° stub-tooth involute	IV	42	1.25	1	1.25	1.96	50.5
	V	54	1	0.8	1	1.57	52.4
	VI	66	0.8	0.64	0.8	1.26	51.52

[a] M is the gear module. D_i is the inner diameter of the stator, which is equal to the diameter of the addendum circle of the ring gear, and is expressed as $D_i = TM - 2A$.

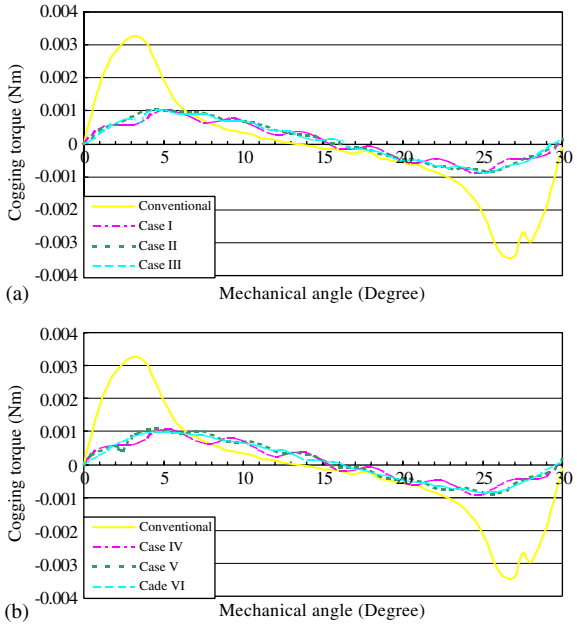

Fig. 7. Distributions of the cogging torques for the proposed motor configurations.

reduction is almost the same for the six cases shown in Table 2, and the peak values of the cogging torque are only 31–33% of the existing product. Furthermore, the gear teeth make the cogging torque distribution smooth especially when the number of gear teeth increases. As can be seen, the proposed motor configuration with gear teeth on the stator experiences a smaller change of the air-gap stored energy than the conventional design as the rotor rotates, and hence reduces the cogging torque.

4. Magnetic circuit analysis and FEM verification

In order to predict the motor performance before fabricating an actual prototype, the analysis of the magnetic field becomes a major concern for motor designers. In general, there are two major approaches for the magnetic field approximations: the magnetic circuit analysis and the finite-element analysis [11]. The magnetic circuit analysis provides the analytical relationships to the

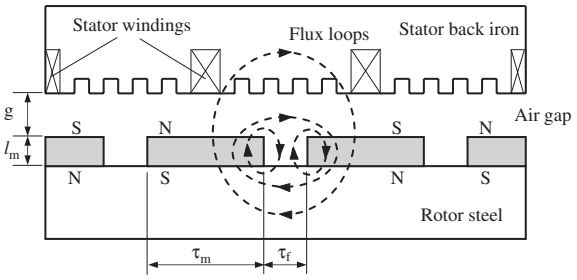

Fig. 8. The linear translational motor topology.

field distribution, magnetic material properties, and machine dimensions, which is of benefit to the machine design and optimization. Comparatively, the finite-element analysis provides the most accurate estimations but is time consuming, which is often used to confirm or improve the results of analytical design works. In this section, a magnetic circuit model taking into account the leakage flux paths around the magnets [12] is used to analytically analyze the magnetic field of the proposed motor with a simplified motor topology. Besides, the two-dimensional FEM is also applied to verify the validity of the magnetic circuit analysis.

Without considering the planetary gear train, the BLDC motor shown in Fig. 4 is a surface-mounted permanent-magnet machine, and the linear translational motor topology is shown in Fig. 8. It is assumed that there is no saturation occurring in the steel region, and the magnetic field intensity produced by the armature current in the stator windings is negligible. Since the magnetic flux density within the air gap directly interacts with the armature current to produce torque, it plays an important role that governs the motor performance. By taking the air-gap leakage flux, magnet-to-magnet leakage flux, and magnet-to-rotor leakage flux into account, the equivalent magnetic circuit of the flux loops shown in Fig. 8 could be set up, and the average flux density within the air gap, $B_{g,ave}$, is obtained [12] as

$$B_{g,ave} = \frac{A_m/A_g}{1 + (R_g/R_{mo})(1 + 2\eta + 4\lambda)} B_r, \quad (12)$$

where A_m/A_g is the ratio of the flux passing area of the magnet to that of the air gap, B_r is the magnet residual flux density, R_g is the air-gap reluctance associated with one magnet pole, R_{mo} is the reluctance of a magnet, η is the reluctance ratio of a magnet pole to the magnet-to-rotor leakage flux, and λ is the reluctance ratio of a magnet pole to the magnet-to-magnet leakage flux, respectively. These factors can be further expressed in terms of magnetic material properties and machine dimensions as follows:

$$A_m = \tau_m L, \tag{13}$$

$$A_g = (\tau_m + \tau_f)L, \tag{14}$$

$$R_{mo} = \frac{l_m}{\mu_0 \mu_r \tau_m L}, \tag{15}$$

$$\eta = \frac{l_m}{\pi \mu_r \tau_m} \ln\left[1 + \frac{\pi \min(g_e, \tau_f/2)}{l_m}\right], \tag{16}$$

$$\lambda = \frac{l_m}{\pi \mu_r \tau_m} \ln\left(1 + \frac{\pi g_e}{\tau_f}\right), \tag{17}$$

$$g_e = \mu_0 \tau_m L R_g, \tag{18}$$

where L is the stack length, τ_m is the magnet width, τ_f is the length of two adjacent magnets, l_m is the magnet height, μ_r is the relative permeability of the magnet, g_e is the effective air-gap length, R_g is the air-gap reluctance, and $\min(g_e,\tau_f/2)$ is the minimum function. For accurate calculating the air-gap reluctance, the presence of the tooth spaces on the stator is taken into account. A simplifying assumption is made that the gear profiles on the stator are rectangular. By utilizing the circular-arc, straight-line permeance model of the gear teeth as shown in Fig. 9, it can be expressed as follows:

$$R_g = \frac{1}{N_t(P_a + 2P_b)}, \tag{19}$$

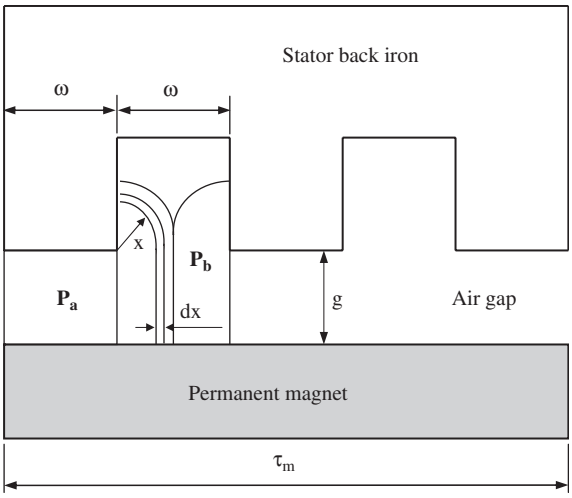

Fig. 9. The circular-arc, straight-line permeance model of the air gap.

where N_t is the number of teeth spaces associated with one magnet pole, and permeances P_a and P_b are given by

$$P_a = \frac{\mu_0 L w}{g}, \tag{20}$$

$$P_b = \int_0^{w/2} \frac{\mu_0 L \, dx}{g + (\pi/2)x} = \frac{2\mu_0 L}{\pi} \ln\left(1 + \frac{\pi w}{4g}\right). \tag{21}$$

Substituting Eqs. (13)–(21) in Eq. (12), the average flux density within the air gap can be obtained, and the back-EMF constant, K_e, and the average electromagnetic torque, T_{ave}, of a BLDC motor [13] are

$$K_e = k_w N B_{g,ave} R_{ro} L, \tag{22}$$

$$T_{ave} = m k_l k_w N B_{g,ave} R_{ro} L i_{ph}, \tag{23}$$

where K_w is the winding factor, N is the total conductors per phase, R_{ro} is the outside rotor radius, m is the phases of conduction, k_l is the correction factor due to losses, and i_{ph} is the phase current, respectively.

Based on the above analytical formulations, the proposed motors with different gear profile systems, numbers of gear teeth, and gear modules shown in Table 2 are analyzed. Table 3 lists the numerical data of the corresponding motor parameters. Table 4 shows the analytical results of the magnetic circuit analysis. Table 5 gives the FEM results and the comparison between the analytical predictions and numerical calculations. The results show that the errors between the FEM results and magnetic circuit analysis are less than 2% for the average air-gap flux density and back-EMF constant, and less than 1% for the average electromagnetic torque. Hence, the analytical results presented above are accurate and suitable for providing further design purposes and optimization.

5. Discussions

Excepting the cogging torque, the average flux density within the air gap, back-EMF constant, average electromagnetic torque, and torque ripple of the BLDC motor are also affected by the gear teeth integrated on the stator. As indicated in Table 4, g_e increases with the gear module, and hence reduces the $B_{g,ave}$. For these six cases, case III which is the 14.5° full-depth involute gear profile system with 66 gear teeth and the gear module equal to 0.8 has the largest $B_{g,ave}$. Considering the values of K_e and T_{ave}, they are proportional to the product of $B_{g,ave}$ and R_{ro}, and also inversely proportional to the summation of the leakage flux λ and η, which does not cross the air gap for interacting with the stator current to produce torque. Hence, Case V which is the 20° stub-tooth involute gear profile system with 54 gear teeth and the gear module equal to 1 performs better than others, but the values are still smaller than the conventional design as shown in

Table 3
Numerical data of the motor parameters

Case	g (mm)	l_m (mm)	τ_m (mm)	τ_f (mm)	L (mm)	R_{ro} (mm)	N_t	n_c[a]	N	i_{ph} (A)
Conventional	0.5	8	33.41	1.15	43	26.00	—	190	760	1.8
I	0.5	8	31.13	1.07	43	24.50	10	190	760	1.8
II	0.5	8	32.65	1.13	43	25.50	13	190	760	1.8
III	0.5	8	32.04	1.10	43	25.10	16	190	760	1.8
IV	0.5	8	31.51	1.07	43	24.75	10	190	760	1.8
V	0.5	8	32.95	1.14	43	25.70	13	190	760	1.8
VI	0.5	8	32.28	1.11	43	25.26	16	190	760	1.8

[a] n_c is the number of coils. For the proposed motor configuration, the number of windings per phase is two and each winding has two groups of conductors, the total conductors per phase can be expressed as $N = 4n_c$.

Table 4
Analytical results of the magnetic circuit analysis for the proposed motor configurations

Case	g_e (mm)	λ (10^{-2})	η (10^{-2})	$B_{g,ave}$ (T)	K_e[a] (V/rad/s)	T_{ave}[a] (Nm)
I	0.5452	7.4313	1.4900	0.1413	0.0979	0.3526
II	0.5317	6.7590	1.4088	0.1418	0.1023	0.3684
III	0.5135	6.8148	1.3906	0.1422	0.1010	0.3636
IV	0.5518	7.3417	1.4884	0.1411	0.0989	0.3559
V	0.5367	6.6967	1.4076	0.1417	0.1031	0.3711
VI	0.5174	6.7635	1.3897	0.1421	0.1016	0.3658

[a] At $k_w = 0.866$, and $k_l = 1$.

Table 5
FEM results and the errors between the FEM results and analytical predictions

Case	FEM results			Error (%)[a]		
	$B_{g,ave}$ (T)	K_e (V/rad/s)	T_{ave} (Nm)	$B_{g,ave}$ (T)	K_e (V/rad/s)	T_{ave} (Nm)
Conventional	0.1411	0.1073	0.3885	—	—	—
I	0.1402	0.0969	0.3533	−0.7846	−1.0320	0.1981
II	0.1404	0.1014	0.3695	−0.9972	−0.8876	0.2977
III	0.1407	0.0998	0.3630	−1.0661	−1.2024	−0.1653
IV	0.1404	0.0982	0.3578	−0.4986	−0.7128	0.5310
V	0.1405	0.1026	0.3735	−0.8541	−0.4873	0.6426
VI	0.1405	0.1007	0.3663	−1.1388	−0.8937	0.1365

[a] Error = (FEM results − Analytical results)/FEM results × 100.

Table 5. This may be due primary to the enlarged effective air gap length and smaller outside rotor radius, which is geometrically constrained by the gear profile system on the stator. It is also noted in Table 4 that the value of λ is larger than that of η for such a surface-mounted permanent-magnet machine. This is because of the small value for τ_f compared with the air-gap length, so that the magnet-to-magnet leakage flux is larger than the magnet-to-rotor leakage flux. As for the torque ripple, which is defined by the difference between the minimum and maximum output torque divided by the average output torque, it is calculated using the FEM and illustrated in Fig. 10. According to the results shown in Table 6, all the six cases possess smaller torque ripple than the conventional design. Case I which is the 14.5° full-depth involute gear profile system with 42 gear teeth and the gear module equal to 1.25 has the lowest torque ripple, although the difference of the torque ripple between them are small.

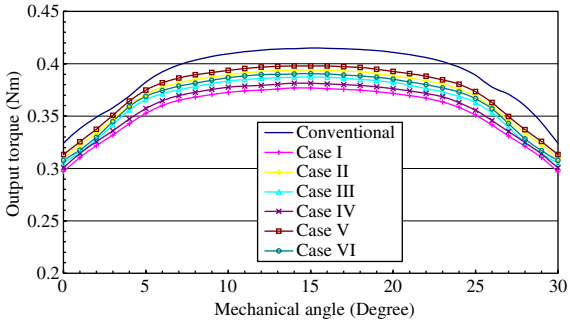

Fig. 10. The distributions of the output torques.

Table 6
Torque ripple calculated using the FEM

Case	Max. torque (Nm)	Min. torque (Nm)	Torque ripple (%)
Conventional	0.4158	0.3240	23.63
I	0.3750	0.2981	21.77
II	0.3929	0.3121	21.87
III	0.3865	0.3073	21.82
IV	0.3807	0.3017	22.08
V	0.3970	0.3144	22.11
VI	0.3904	0.3096	22.06

6. Conclusion

A novel configuration of a BLDC motor with an integrated planetary gear train has been presented, which overcomes the inherent shortcomings of traditional designs. The special feature of the proposed design lies in the integration of the standard gear profile systems on the stator. It simplifies the mechanical elements and makes the whole configuration more compact and easier for maintenance. From the functional point of view, the gear teeth provides not only for transmission, but also for cogging torque reduction. The relationships to the number of gear teeth, the number of magnet poles, and the orders of harmonic components that generate the cogging torque are investigated, while two gear profile systems with standard gear modules and feasible numbers of gear teeth are presented for reducing the cogging torque. The magnetic circuit approach with the corresponding air-gap permeance model is applied to analytically analyze the magnetic field of the proposed motor, which is suitable for further design purposes and optimization. Furthermore, the validity is verified by the FEM. Among the six proposed cases, it shows that Case III has the largest average flux density within the air gap, while Case V possesses the largest back-EMF constant and the average electromagnetic torque. As for the torque ripple, Case I performs better than others. Due to the characteristics of lower cogging torque and torque ripple compared with the conventional design, the proposed configuration is beneficial for the accurate motion and position control of BLDC motors.

Acknowledgments

The authors are grateful to the National Science Council (Taiwan, ROC) for supporting this research under Grant NSC93-2212-E-006-091. Also, they would like to thank the Electric Motor Technology Research Center and Prof. M. C. Tsai of the Department of Mechanical Engineering, National Cheng Kung University, Taiwan, for the supporting of the Ansoft/Maxwell software on this research.

References

[1] B. Fahimi, A. Emadi, R.B. Sepe Jr., IEEE Trans. Energy Conver. 19 (1) (2004) 116.
[2] K. Suzuki, Y. Inaguma, K. Haga, T. Nakayama, Society of automotive engineers, Paper no. 950580, 1995, p. 948.
[3] N.C. Harris, T.M. Jahns, S. Huang, Proceedings of IEEE Industry Applications Society Annual Meeting, vol. 3, Pittsburgh, PA, 2002, p. 2028.
[4] S. Kinoshita, K. Sakagami, U.S. Patent 6,031,308, 2000.
[5] K. Minegishi, J. Tamenaga, U.S. Patent 6,485,394, 2002.
[6] M. Goto, K. Kobayashi, Electr. Eng. Jpn. 103 (5) (1983) 113.
[7] S.M. Hwang, J.B. Eom, G.B. Hwang, W.B. Jeong, Y.H. Jung, IEEE Trans. Magn. 36 (5) (2000) 3144.
[8] C.S. Koh, J.S. Seol, IEEE Trans. Magn. 39 (6) (2003) 3503.
[9] F. Tajima, H. Katayama, K. Miyashita, T. Tamura, K. Hironaka, T. Kawano, Y. Sekita, K. Saito, A. Tamura, US Patent 4,672,253, 1987.
[10] C.E. Wilson, J.P. Sadler, Kinematics and Dynamics of Machinery, HarperCollins College Publishers, New York, 1993.
[11] D.C. Hanselman, Brushless Permanent-Magnet Motor Design, McGraw-Hill, New York, 1994.
[12] R. Qu, T.A. Lipo, IEEE Trans. Ind. Appl. 40 (1) (2004) 121.
[13] M.C. Tsai, M.H. Weng, M.F. Hsieh, IEEE Trans. Magn. 38 (5) (2001) 3467.